Journal of Controlled Release 388 (2025) 114314

Contents lists available at ScienceDirect

Journal of Controlled Release

journal homepage: www.elsevier.com/locate/jconrel

Claudin 5-binding small molecule transiently opens the blood-brain barrier and safely enhances brain drug delivery

Saito Inoue [a,1], Keisuke Shirakura [a,1], Atsuya Shirono [a,1], Jumpei Taguchi [b], Yoshiki Ikeda [c], Satomi Tomita [b], Risa Funatsu [a], Kosuke Muraoka [a], Yosuke Hashimoto [a], Keisuke Tachibana [a], Nobumasa Hino [a,d], Takefumi Doi [a], Yui Ikemi [a], Kazuto Nunomura [a], Bangzhong Lin [a], Shinsaku Nakagawa [a], Kazutake Tsujikawa [a], Shota Tanaka [a], Masanori Obana [a,d,e], Yasushi Fujio [a,d,e], Takamitsu Hosoya [b], Hiroyuki Takeda [f,**], Masuo Kondoh [a,d,*], Yoshiaki Okada [a,d,*]

[a] Graduate School of Pharmaceutical Sciences, The University of Osaka, Osaka 565-0871, Japan
[b] Chemical Bioscience Team, Laboratory for Biomaterials and Bioengineering, Institute of Integrated Research, Institute of Science Tokyo, Tokyo 101-0062, Japan
[c] Institute for Integrated Cell-Material Sciences, Kyoto University, Kyoto 606-8501, Japan
[d] Center for Infectious Disease Education and Research, The University of Osaka, Osaka 565-0871, Japan
[e] Integrated Frontier Research for Medical Science Division, Institute for Open and Transdisciplinary Research Initiative, The University of Osaka, Osaka 565-0871, Japan
[f] Proteo-Science Center, Ehime University, Ehime 790-8577, Japan

ARTICLE INFO

Keywords:
Blood–brain barrier
Drug delivery
Claudin 5
Tight junction
Permeability

ABSTRACT

The blood–brain barrier (BBB) protects the brain from harmful substances, but it also limits drug delivery, hindering the treatment of brain diseases. Claudin 5, a tight junction protein in endothelial cells, plays a key role in maintaining the BBB integrity. Although modulation of Claudin 5 is a promising strategy for transiently opening the BBB, the currently available modulators often cause adverse effects due to strong or prolonged activity. Thus, we aimed to develop a moderate Claudin 5 modulator that enables safe and transient opening of the BBB. We identified a Claudin 5-binding small molecule (CL5B), capable of binding Claudin 5 via a high-throughput screening of 9600 compounds using a Claudin 5 antibody and proteoliposomes. CL5B increased endothelial permeability and tracer permeation across the endothelial monolayer by altering the localization of Claudin 5 without affecting its expression. In mice, CL5B transiently opened the BBB for less than 30 min, delivering drugs specifically to the brain. Notably, CL5B-facilitated delivery of methylscopolamine, a drug with limited brain penetration, alleviated seizure symptoms in a mouse epilepsy model. These findings demonstrate that CL5B is a safe BBB modulator that enhances brain drug delivery and holds therapeutic potential for brain diseases.

1. Introduction

Considering the global surge in aging population, novel drugs are required for treating brain diseases; however, the development of effective drugs remains challenging. One of the main difficulties in brain drug discovery is the presence of the blood–brain barrier (BBB) in cerebral blood vessels, which restricts the passage of harmful substances from the blood to the brain [1]. Although the BBB is essential for protecting the brain, it prevents drug delivery, thereby impeding the development of drugs for brain diseases. Therefore, it is crucial to develop technologies that can modulate the BBB function and enhance drug delivery to the brain.

Endothelial cells (ECs) cover the inner surface of blood vessels. ECs in the brain capillaries strictly seal the intercellular spaces through tight junctions. Tight junctions are composed of several transmembrane and scaffolding proteins, including claudins (CLDNs), occludin, and ZO-1

* Corresponding authors at: Graduate School of Pharmaceutical Sciences, The University of Osaka, Osaka 565-0871, Japan.
** Corresponding author.
E-mail address: okadabos@phs.osaka-u.ac.jp (Y. Okada).
[1] These authors contributed equally to the present study.

https://doi.org/10.1016/j.jconrel.2025.114314
Received 22 July 2025; Received in revised form 8 October 2025; Accepted 10 October 2025
Available online 11 October 2025

[2]. CLDNs are integral membrane proteins characterized by four transmembrane domains, extracellular oligomerization domains, and intracellular domains [3–5]. The paracellular sealing function of CLDNs is mediated by the extracellular domains at EC junctions [3,6,7]. Claudin 5 (CLDN5), an endothelium-enriched CLDN, plays a crucial role in maintaining the BBB function. Genetic deletion or pharmacological inhibition of CLDN5 in mice [8–10] and zebrafish [11] impairs the BBB and enhances the delivery of tracers to the brain. These findings highlight the essential role of CLDN5 in the BBB function [12], and indicate that CLDN5 modulation can be a potential strategy for enhancing drug delivery to the brain.

Small-interfering RNAs (siRNAs) [13,14] and a small molecule (M01) [15] that decrease CLDN5 levels were developed for modulating the BBB via CLDN5. In addition, derivatives of the nontoxic C-terminal domain of *Clostridium perfringens* enterotoxin (cCPE) [16–19], CLDN5 extracellular loop peptides [18,20,21], and CLDN5 antibodies [22,23] that modulate CLDN5 function by binding to its extracellular domain were also developed. These CLDN5 modulators increase the endothelial permeability and enhance the delivery of drugs (smaller than 1 kDa) to the brain in mice and cynomolgus monkeys [13,15,20,24], suggesting that CLDN5 modulation can serve as a strategy for drug delivery to the brain. However, this strategy is potentially risky. For instance, injection of a CLDN5 antibody caused edema in the brain and lungs of animals, presumably due to its strong and prolonged effect [24,25]. Also, CLDN5 knockout in mice induced severe vascular leakage of larger molecules (10 kDa) in the brain and lethal neuroinflammation [8,10]. These reports suggest that strong and persistent CLDN5 inhibition induces excessive vascular hyperpermeability, exerting severe adverse effects. Therefore, it is important to develop moderate CLDN5 modulators that can control and minimize the duration of BBB opening for establishing

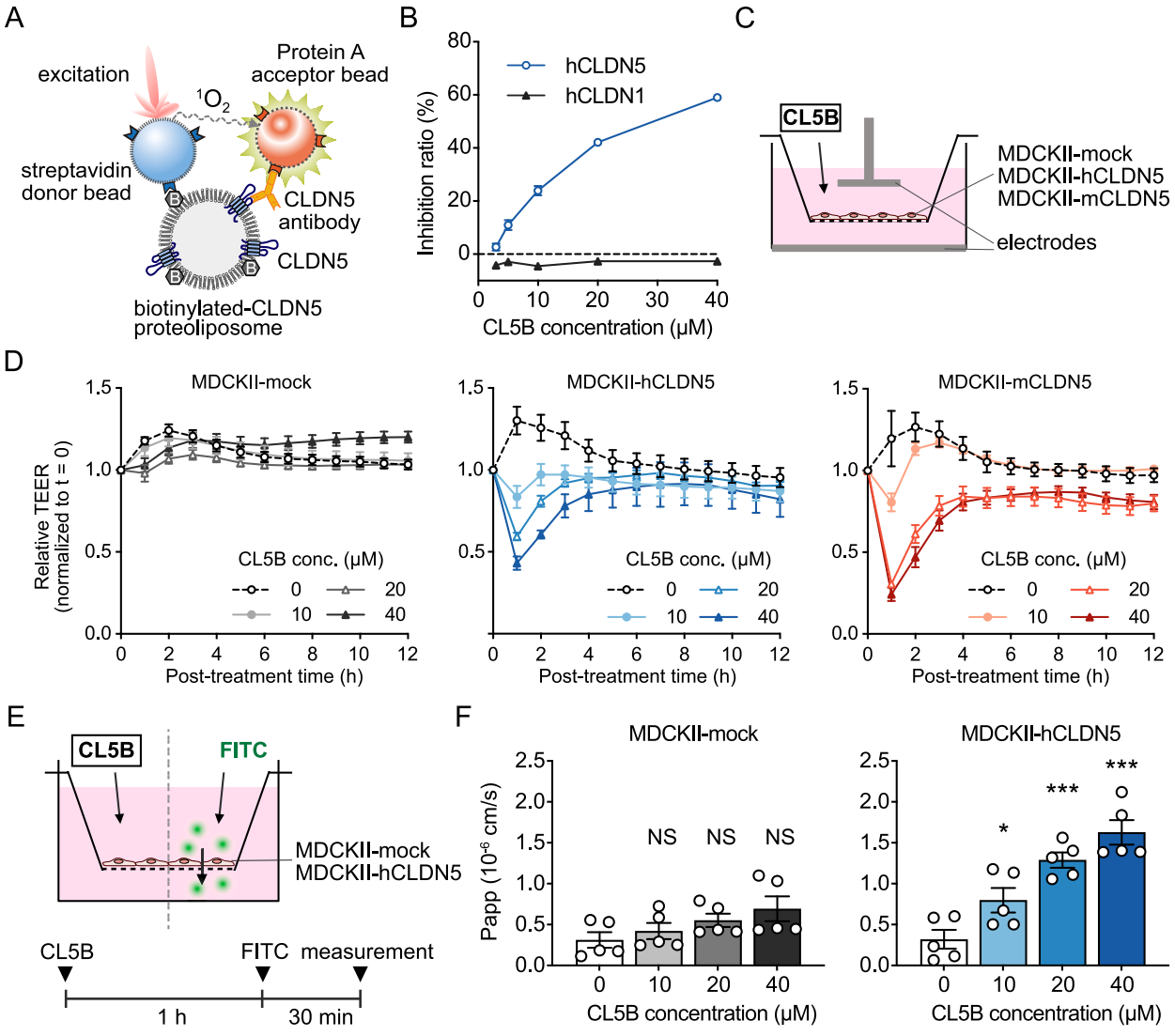

Fig. 1. Screening of small CLDN5-binding molecules.
(A) The screening system for CLDN5-binding molecules using the biotinylated-hCLDN5 proteoliposome and hCLDN5 antibody (Ab). When hCLDN5 Ab binds to hCLDN5, a chemiluminescence signal is generated through $^1O_2$ transfer from the donor to the acceptor beads. The signal is suppressed when compounds bind to CLDN5 and inhibit its interaction with the CLDN5 Ab. The same screening system was generated using CLDN1 Ab and CLDN1-binding liposome to identify CLDN5-specific binding molecules. (B) CL5B-mediated inhibition of the chemiluminescence signal in the screening system for CLDN5 but not CLDN1. (C) The measurement system for transepithelial-electrical resistance (TEER) using MDCKII cells. The TEER for MDCKII cell monolayer on cell culture inserts was measured with or without CL5B treatment. (D) Effect of CL5B on cell permeability. MDCKII-mock, MDCKII-hCLDN5, and MDCKII-mCLDN5 cells were treated with CL5B or left untreated, and the TEER was measured (mock and hCLDN5: $n = 5$; mCLDN5: $n = 4$). (E) Schematic illustration of the tracer permeation assay. MDCKII-mock and MDCKII-hCLDN5 cells in cell culture inserts were treated with CL5B for 1 h or left untreated, and fluorescein isothiocyanate (FITC) permeation was measured. (F) Effect of CL5B on FITC permeation through cell monolayers (mock and hCLDN5: $n = 5$; mCLDN5: $n = 5$). $^{**}P < 0.01$ by Dunnett's multiple comparisons test.

safe and clinically applicable brain drug delivery systems.

In this study, we searched for a small molecule that can bind to CLDN5 and moderately inhibit its function. Using a unique screening system with a CLDN5 antibody and proteoliposomes, we identified a CLDN5-binding small molecule (CL5B). CL5B reversibly increased the endothelial permeability. Furthermore, it promoted the delivery of drugs to the brain by transiently opening the BBB within 30 min and ameliorated epileptic seizures in a mouse model. Thus, we successfully identified CL5B as a moderate CLDN5 modulator that transiently opens the BBB and safely delivers drugs to the brain.

2. Results

2.1. Screening of hCLDN5-binding small molecules

To obtain small molecule-based CLDN5 binders with moderate BBB regulatory activity, we established a screening system using a human CLDN5 (hCLDN5) proteoliposome and an hCLDN5 antibody M48 [22] that recognizes the tertiary structure of the second extracellular loop of human CLDN5 (ECL2) (Fig. 1A). Using this system, we screened a chemical library of 9600 compounds and selected compounds that inhibited the binding between hCLDN5 and M48. To evaluate concentration dependence of inhibition, the selected compounds were tested in the same assay system at five concentrations. Simultaneously, an assay using CLDN1 and an antibody against it was performed to eliminate false positives. We identified a CLDN5-binding small molecule (CL5B) that inhibited the interaction between CLDN5 and its antibody in a specific and dose-dependent manner (Fig. 1B). Analysis of CL5B function revealed that CL5B treatment transiently and dose-dependently decreased transepithelial/endothelial electrical resistance (TEER) in a monolayer of Madin-Darby canine kidney II (MDCKII) cells expressing human or mouse CLDN5 (mCLDN5; MDCKII-hCLDN5/-mCLDN5), but

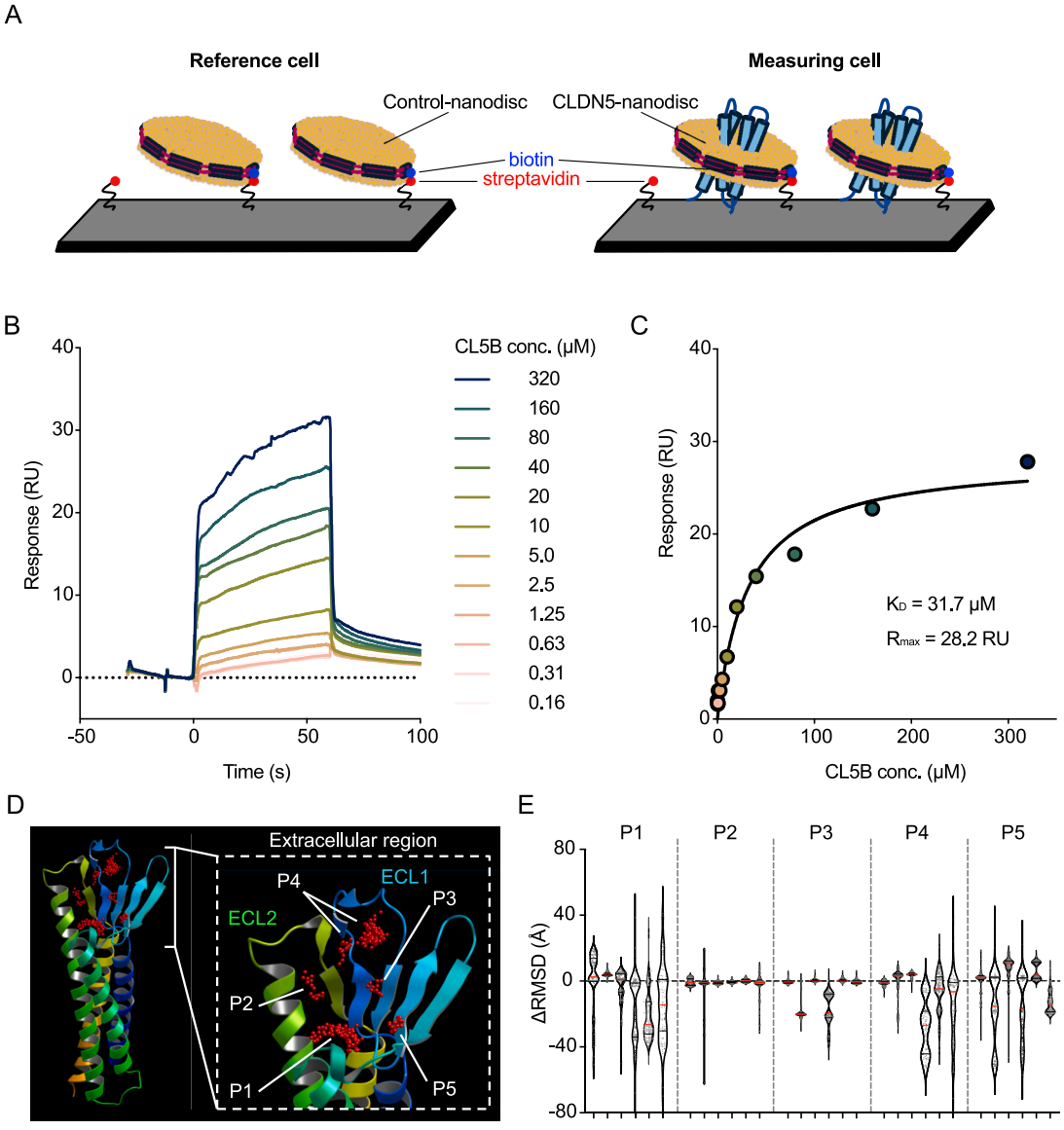

Fig. 2. Interaction between CL5B and CLDN5.
(A) Immobilization of nanodiscs on a Sensor Chip SA. Nanodiscs were captured by streptavidin on the SA chip via biotinylated MSP. (B) Representative double-referenced sensorgram of the interaction between CLDN5-nanodiscs and CL5B. (C) Representative saturation curve of steady-state binding responses. (D) Potential CL5B-binding pockets in the CLDN5 extracellular region. The five pockets (P1 to P5) predicted using the MolSite method and extracellular loops of CLDN5 (ECL1/2) are indicated. (E) Analysis of the binding stability of CL5B to each pocket. Molecular dynamics simulations were performed ($n = 6$ per pocket). Each lane shows the change in root mean square deviation (ΔRMSD) values (subtracted RMSD of 0 ns to each trajectory point), which indicate the distance moved from the initial position of CL5B placed in each pocket.

not in the MDCKII-mock cell monolayer (Fig. 1C, D). Consistent with this, CL5B treatment increased the passage of a small fluorescent tracer (fluorescein isothiocyanate (FITC); 389 Da) through a layer of MDCKII-hCLDN5 cells but not of MDCKII-mock cells (Fig. 1E, F). These results indicated that CL5B enhanced the permeability of MDCKII cell layers in a manner dependent on human and mouse CLDN5.

2.2. Analysis of the binding between CL5B and hCLDN5

To confirm the interaction between CL5B and hCLDN5, a surface plasmon resonance (SPR) assay was performed. Biotinylated nanodiscs with hCLDN5 (CLDN5-nanodiscs) and ones without hCLDN5 (Control-nanodiscs) were immobilized on the measuring and reference cells in streptavidin coated SPR sensor chip, respectively (Fig. 2A). To evaluate the binding affinity, serial dilutions of CL5B were injected over the sensor surface, and dissociation constant (K_D) and maximum analyte response (R_{max}) were determined by plotting a saturation curve from the steady-state response values at each concentration (Fig. 2B, C). We conducted four independent experiments using two different production lots of CLDN5-nanodiscs (two experiments per lot), and in all cases, CL5B exhibited concentration-dependent binding to the CLDN5-nanodiscs. The K_D ranged from 31.7 to 58.3 μM. These results indicated that CL5B binds directly to hCLDN5.

To identify the potential CL5B-binding pocket in hCLDN5, we performed an in silico analysis. We retrieved the predicted structure of human CLDN5 from the AlphaFold Protein Structure database (https://alphafold.ebi.ac.uk, ID: AF-O00501-F1-v4), searched for binding pockets in the extracellular region of CLDN5 using the Molsite method and identified five pockets (P1–P5) (Fig. 2D). Docking pose prediction was performed with CL5B, and binding stability was analyzed six times using molecular dynamics simulation (Fig. 2E, Fig. S1). The change in root mean square deviation (ΔRMSD) values, which indicate the distance moved from the initial position of CL5B placed in each pocket, showed significant changes in P1, P4, and P5, but not in P2 and P3. Consistently, in P2 and P3, the number of contacts was higher, and the minimum distance values were lower than those in P1, P4, and P5

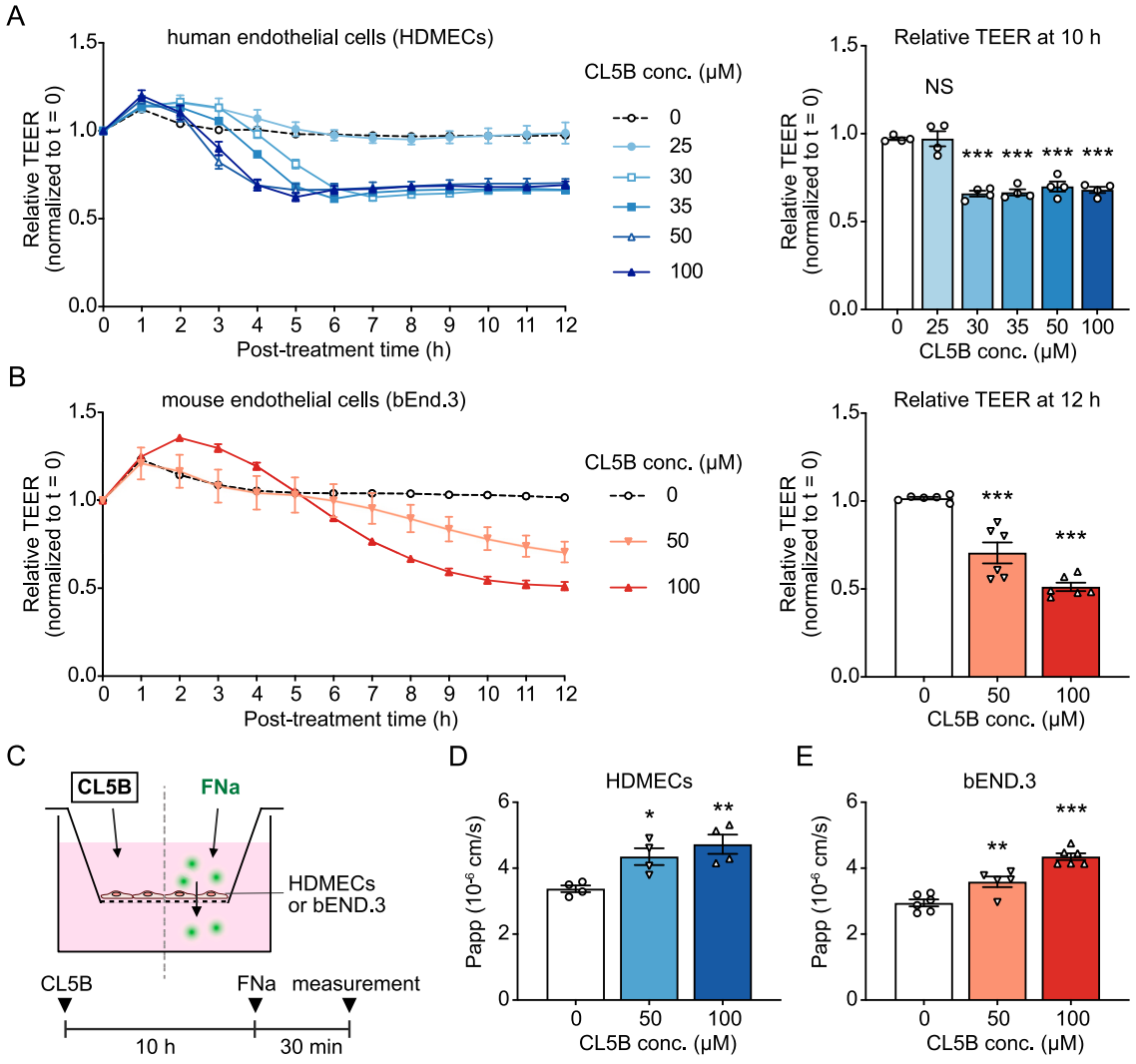

Fig. 3. CL5B enhances endothelial permeability and promotes small-molecule permeation.
(A) Effect of CL5B on human EC permeability. A monolayer of human microvascular ECs (HDMECs) expressing endogenous CLDN5 in the cell culture insert was treated with CL5B or left untreated, and the trans-endothelial electrical resistance (TEER) was measured. The graph on the right indicates the TEER at 10 h ($n = 4$). $^*P < 0.05$, $^{**}P < 0.01$, $^{***}P < 0.001$ by Dunnett's multiple comparisons test. (B) Effect of CL5B on mouse brain EC permeability. A monolayer of bEnd.3 (a mouse brain EC line) in cell culture inserts was treated with CL5B or left untreated, and the TEER was measured. The graph on the right indicates the TEER at 12 h ($n = 6$). $^*P < 0.05$, $^{**}P < 0.01$, $^{***}P < 0.001$ by Dunnett's multiple comparisons test. (C) Schematic illustration of the tracer permeation assay. HDMECs or bEnd.3 cells in cell culture inserts were treated with CL5B for 1 h or left untreated, and sodium fluorescein (FNa) permeation was measured. (D and E) Effect of CL5B on FNa permeation through monolayers of HDMECs ($n = 4$; D) and bEnd.3 ($n = 5$; E). $^*P < 0.05$, $^{**}P < 0.01$ by Dunnett's multiple comparisons test.

(Fig. S1). Comparing P2 and P3, the number of contacts in P2 was higher than that in P3 (Fig. S1). Although CL5B was dislodged from both P2 and P3 twice in the six simulations, CL5B stayed longer in P2 than in P3 (Fig. 2E, Fig. S1, Supplementary video 1). These results suggest that CL5B can stably bind to P2, close to ECL2 of CLDN5.

2.3. CL5B increases the permeability of endothelial monolayers

To investigate the effects of CL5B on endothelial permeability, we treated human primary ECs, expressing endogenous CLDN5, with CL5B and measured the TEER. CL5B treatment decreased the TEER in human microvascular ECs in a dose-dependent manner (Fig. 3A). Consistently, CL5B treatment enhanced the passage of sodium fluorescein (FNa; 376 Da) through the EC monolayers (Fig. 3C, D). In addition, CL5B treatment dose-dependently decreased the TEER in the mouse brain EC line, bEnd.3 (Fig. 3B) and enhanced FNa passage through the monolayers (Fig. 3E). These results indicated that CL5B promotes tracer delivery through human and mouse EC monolayers by enhancing their permeability.

2.4. Mechanistic analysis of CL5B-mediated endothelial permeability

To investigate whether CL5B increases endothelial permeability by inhibiting CLDN5, we performed siRNA-mediated knockdown experiments. After confirming the CLDN5 siRNA-mediated decrease in CLDN5 protein expression (Fig. 4A), we measured TEER in ECs treated with or without CL5B. CL5B decreased the TEER in ECs transfected with Control siRNA, but not in those transfected with CLDN5 siRNA (Fig. 4B). In addition, the CL5B-mediated decrease in the TEER was recovered by depleting CL5B from the medium (Fig. 4C). These results indicated that CL5B reversibly enhances endothelial permeability in a CLDN5-dependent manner.

To further investigate how CL5B enhances endothelial permeability, CLDN5 localization was analyzed in CL5B-treated ECs. CL5B treatment induced discontinuous CLDN5 localization at the EC junctions, whereas CLDN5 was continuously localized at the junctions in nontreated cells (Fig. 4D). Quantitative analysis indicated that treatment with CL5B decreased the CLDN5 localized at the intercellular junctions from 73.6 % to 35.7 % in ECs. Furthermore, super-resolution microscopic analysis revealed CL5B-induced intercellular gaps with discontinuous CLDN5 localization (Fig. 4E). In addition, CL5B treatment did not alter the CLDN5 expression at protein and mRNA levels (Fig. 4F, G) or the mRNA expression of other endothelial junction proteins, including ZO-1, Occludin, and VE-cadherin (Fig. 4G). These results suggest that CL5B increases endothelial permeability by modulating the localization of CLDN5 at cell junctions.

2.5. CL5B regulates mouse BBB and promotes drug delivery to the brain

To investigate the effects of CL5B on the BBB, wild-type mice were intravenously coinjected with CL5B and fluorescent tracers (Fig. 5A). CL5B promoted FNa delivery to the brain (Fig. 5B), which indicated that it opens the mouse BBB and enhances the delivery of the tracer to the brain.

To evaluate the effect of CL5B on hCLDN5 in the BBB, we employed hCLDN5 knock-in mice (hCLDN5-KI mice), in which the coding sequence of mCLDN5 was replaced with that of hCLDN5, and analyzed whether the mice could be used for evaluating hCLDN5 modulators. Organ distribution of h*CLDN5* in the hCLDN5-KI mice was comparable to that of m*CLDN5* in wild-type mice (Fig. S2A). In hCLDN5-KI mice, a hCLDN5 antibody (R9) [22], which is a known hCLDN5 modulator that recognizes hCLDN5 but not mCLDN5, could bind to the brain vasculature (Fig. S2B) and enhanced bran delivery of FNa but not of a larger tracer, FITC-dextran (FD4; 4 kDa) (Fig. S2C–E). These results indicated that hCLDN5-KI mice can be used to evaluate BBB modulators that bind to hCLDN5.

To investigate whether CL5B regulates hCLDN5 in the BBB, hCLDN5-KI mice were intravenously injected with CL5B and fluorescent tracers (Fig. 5A). Upon simultaneous injection with CL5B, FNa was delivered to the brain (Fig. 5C). However, when FNa was injected 30 min after CL5B injection, FNa was not delivered to the brain (Fig. 5D), indicating that the duration of CL5B-mediated BBB opening was less than 30 min. Notably, analysis of blood samples from CL5B-injected mice revealed a rapid decrease in CL5B concentration within 20 min (Fig. 5E, Fig. S3), suggesting that CL5B-mediated short-term opening of the BBB was due to its rapid removal from the blood. In addition, analysis of FNa delivery to other organs revealed that CL5B enhanced FNa delivery specifically to the brain (Fig. 5F). These results indicated that CL5B rapidly and transiently opens the BBB by targeting both human and mouse CLDN5 and facilitates the delivery of a tracer specifically to the brain.

We further investigated whether CL5B can promote the delivery of other tracers and drugs to the brain. CL5B promoted the delivery of Hoechst33258 (533 Da), methylscopolamine (MSco; 318 Da), and vancomycin (1.4 kDa), which were otherwise barely delivered to the brain, but not of FD4 (Fig. 5G-J). These results suggest that CL5B can promote the delivery of various molecules to the brain without inducing excessive BBB opening that allows permeation of larger molecules.

2.6. CL5B enhanced drug delivery and suppressed brain disease in mice

To investigate whether CL5B promotes drug delivery to the brain and alleviates brain disease, we generated a mouse epileptic seizure model by intraperitoneally injecting pilocarpine (a muscarinic receptor agonist) into wild-type mice pretreated with MSco to antagonize peripheral muscarinic receptors (Fig. 6A). In this model, pilocarpine induced epileptic seizures mainly through brain muscarinic receptors and not through peripheral receptors. Coinjection of CL5B and MSco reduced the mortality in the epilepsy model mice compared with that in the nontreated, CL5B-treated, or MSco-treated mice (Fig. 6B). Consistently, the evaluation of seizure intensity according to the Racine scale revealed that coinjection of CL5B and MSco efficiently suppressed the seizure intensity in mice compared with that in mice injected with either CL5B or MSco or in those that were not injected (Fig. 6C-E). These results indicated that CL5B enhanced the delivery of MSco to the brain and suppressed pilocarpine-induced epileptic seizures.

3. Discussion

CLDN5 modulators, including CLDN5-suppressing molecules (such as siRNAs and small molecules) and CLDN5-binding molecules (such as peptides and antibodies), have been reported to open the BBB for a period of several hours to a few days and enhance drug delivery to the brain without causing significant adverse effects [13,15,20]. However, recent studies have demonstrated that prolonged CLDN5 suppression, either via long-term siRNA treatment or conditional knockout in adult mice over several weeks, leads to the development of brain disorders [8,10]. These findings suggest that shortening the CLDN5 modulator-mediated BBB opening duration to less than a few hours may maximize the safety of drug delivery to the brain. Moreover, a highly potent anti-CLDN5 antibody was reported to induce edema and vascular dilation in multiple organs [24,25], indicating that activity of CLDN5 modulators must be moderate to avoid excessive disruption of CLDN5-mediated junctions in organs. Based on this evidence, we surmised that moderate CLDN5 modulators that transiently open the BBB—ideally for less than one hour—should be safe BBB regulators for drug delivery to the brain. To discover such modulators, we screened small-molecule CLDN5 binders and identified CL5B. CL5B transiently opened the BBB within 30 min, allowed the delivery of drugs specifically to the brain, and ameliorated epileptic seizures in mice. These findings indicate that CL5B is a promising and safe enhancer of brain drug delivery with potential for therapeutic applications in brain diseases.

In addition to the brain vasculature, CLDN5 is also expressed in the

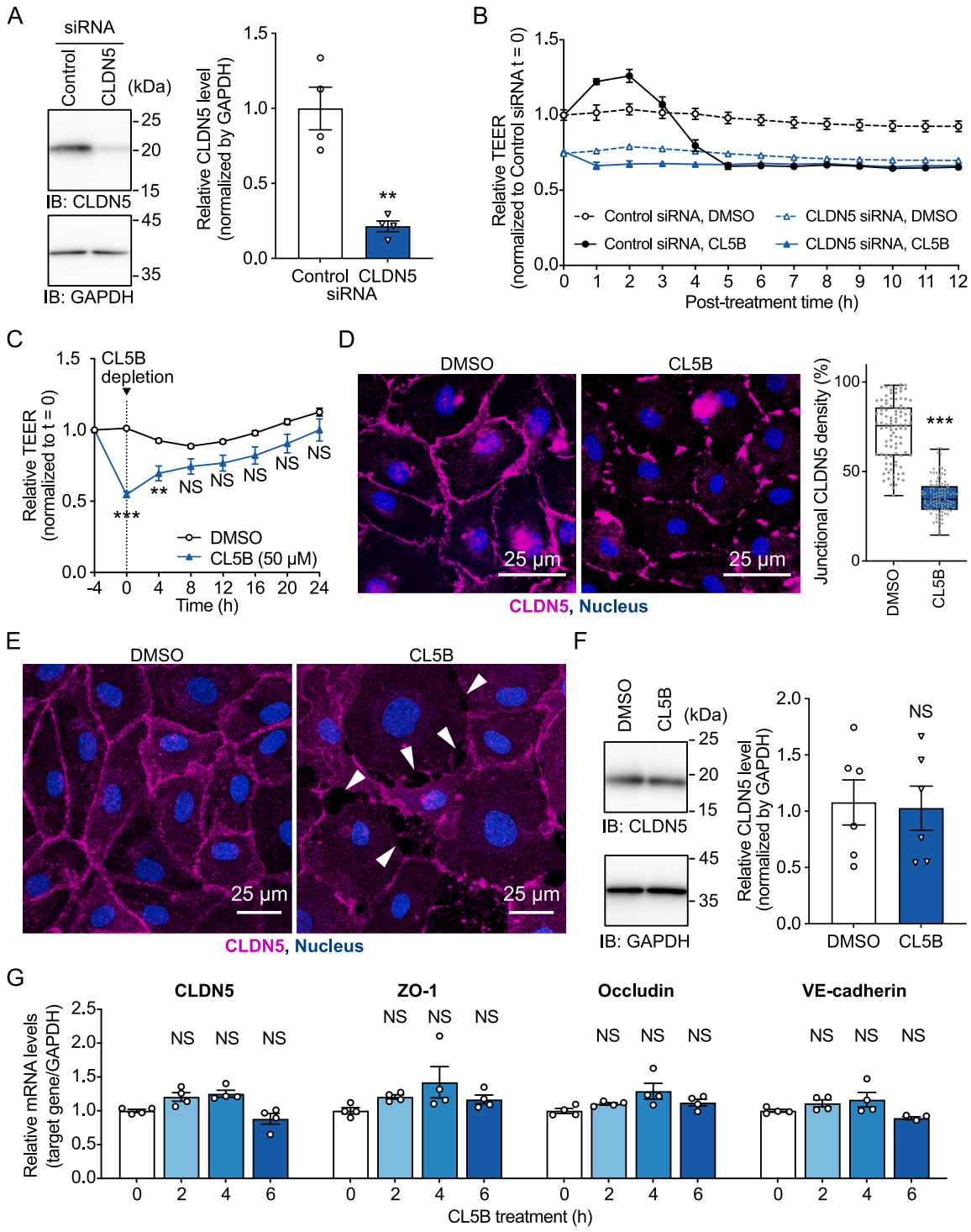

Fig. 4. CL5B reversibly enhances endothelial permeability by altering CLDN5 localization.
(A) CLDN5 expression level in HDMEC transfected with siRNA. HDMECs were transfected with control or CLDN5 siRNA, and CLDN5 protein levels were analyzed using western blotting. GAPDH was used as an internal control. (n = 4) $^{**}P < 0.01$ by Welch's *t*-test. (B) Effect of CL5B on permeability in CLDN5-downregulated ECs. HDMECs were transfected with siRNA for CLDN5 or control, treated with CL5B or left untreated, and used for TEER measurements ($n = 4$). (C) Effects of CL5B depletion on endothelial permeability. HDMEC monolayers were treated with CL5B. After 4 h, CL5B was depleted, and TEER was measured ($n = 5$). NS: not significant; $^{**}P < 0.01$, $^{***}P < 0.001$ by Bonferroni's multiple comparisons test. (D) CLDN5 localization in CL5B-treated ECs. HDMECs were treated with CL5B for 10 h and subjected to immunofluorescent staining for CLDN5 ($n = 100$ cells from five images). $^{***}P < 0.001$ by Mann–Whitney *U* test. (E) Super-resolution microscopic images of CLDN5 localization and intercellular gaps induced by CL5B. HDMECs treated with or without CL5B were stained for CLDN5 and observed using super-resolution microscopy. (F) The protein levels of CLDN5 in CL5B-treated ECs. HDMECs were treated with CL5B for 10 h and then used for western blotting. GAPDH was used as an internal control ($n = 6$). NS: not significant by Welch's *t*-test. (G) Effect of CL5B on endothelial junction-related molecules. HDMECs were treated with CL5B for 2, 4, or 6 h or left untreated, and mRNA levels of *CLDN5*, *ZO-1*, occludin, and VE-cadherin were measured using qRT-PCR ($n = 4$). NS: not significant by Kruskal–Wallis one-way ANOVA followed by Dunn's multiple test (vs. 0 h).

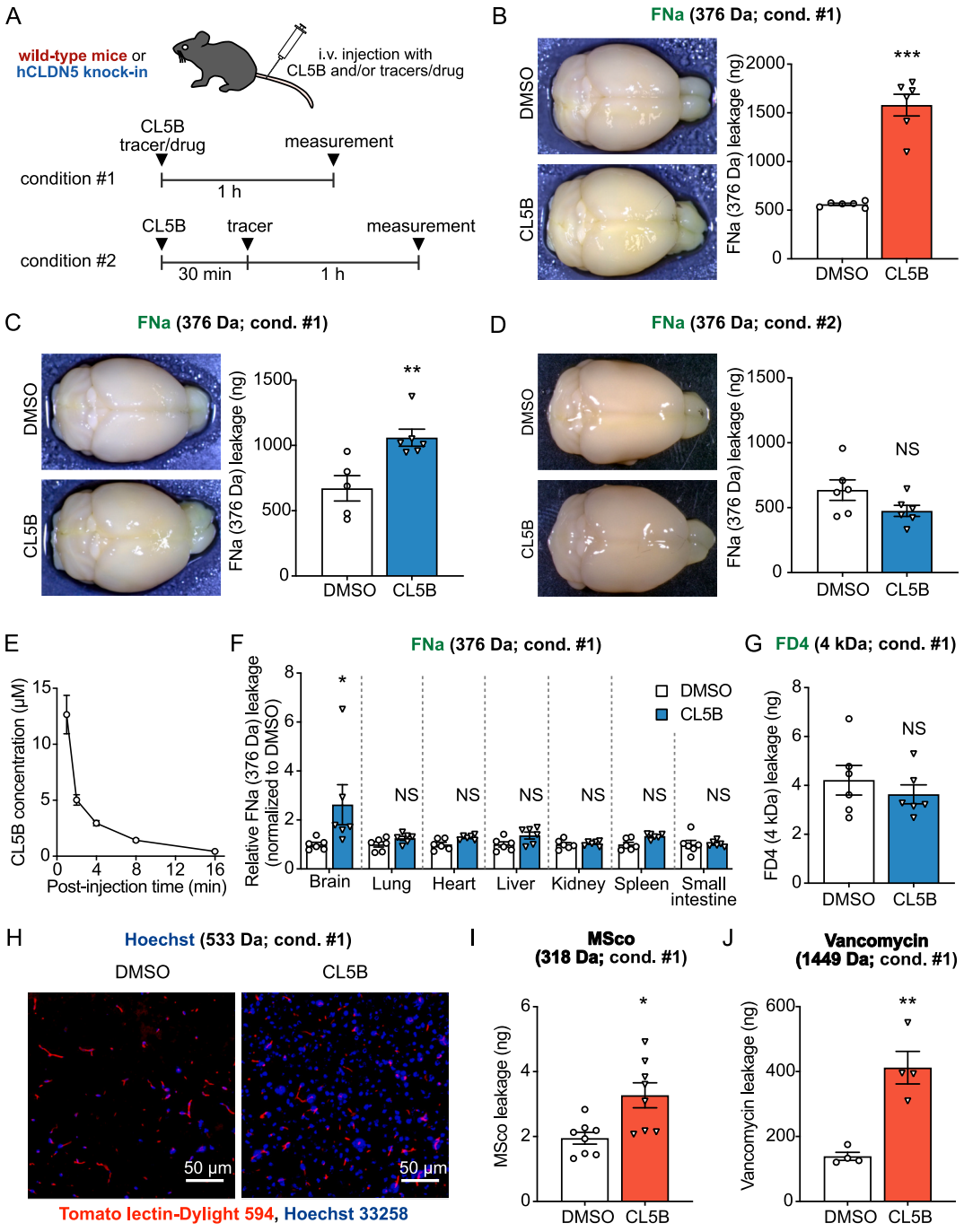

Fig. 5. CL5B enhances brain drug delivery by transiently opening the BBB.
(A) Schematic illustration of brain tracer delivery assays. hCLDN5-KI or wild-type mice were intravenously injected with fluorescent tracers in the presence or absence of CL5B under two different conditions (condition #1 and condition #2). (B) FNa delivery assay using wild-type mice. Wild-type mice were injected with FNa and CL5B, and the extravasated FNa in the brains was quantified ($n = 6$). Images are of the representative brains used for the assay. ***$P < 0.001$ by Welch's *t*-test. (C and D) FNa delivery assay. hCLDN5-KI mice were injected with FNa and CL5B under condition #1 (C) and #2 (D). Extravasated FNa levels in the brain were measured ($n = 6$). Images are of the representative brains used for the assay. **$P < 0.01$; NS: not significant by Mann–Whitney *U* test (C) and Welch's *t*-test (D). (E) CL5B concentration in blood of CL5B-injected mice. Blood samples were collected from CL5B-injected wild-type mice, and CL5B concentration was measured by mass spectrometry. (F) CL5B-mediated FNa delivery to various organs. hCLDN5-KI mice were injected with FNa and CL5B, and the extravasated FNa in each organ was measured ($n = 6$). *$P < 0.001$; NS: not significant by Mann–Whitney *U* test. (G) FD4 delivery assay. hCLDN5-KI mice were injected with FD4 and CL5B, and the extravasated FD4 in the brain was quantified ($n = 6$). Images are of the representative brains used for the assay. NS: not significant by Welch's *t*-test. (H) Tracer delivery assay using a fluorescent molecule, Hoechst 33258 (533 Da). hCLDN5-KI mice injected with Hoechst 33258 and CL5B. Blood vessels were stained by injecting Dylight594-labeled tomato lectin. (I and J) Drug delivery assay using methylscopolamine (318 Da) (H) and vancomycin (1449 Da) (I). Wild-type mice were injected with CL5B together with methylscopolamine ($n = 8$; I) or vancomycin ($n = 4$; J). The extravasated methylscopolamine and vancomycin were measured using LC/MSMS. *$P < 0.05$ by Welch's *t*-test.

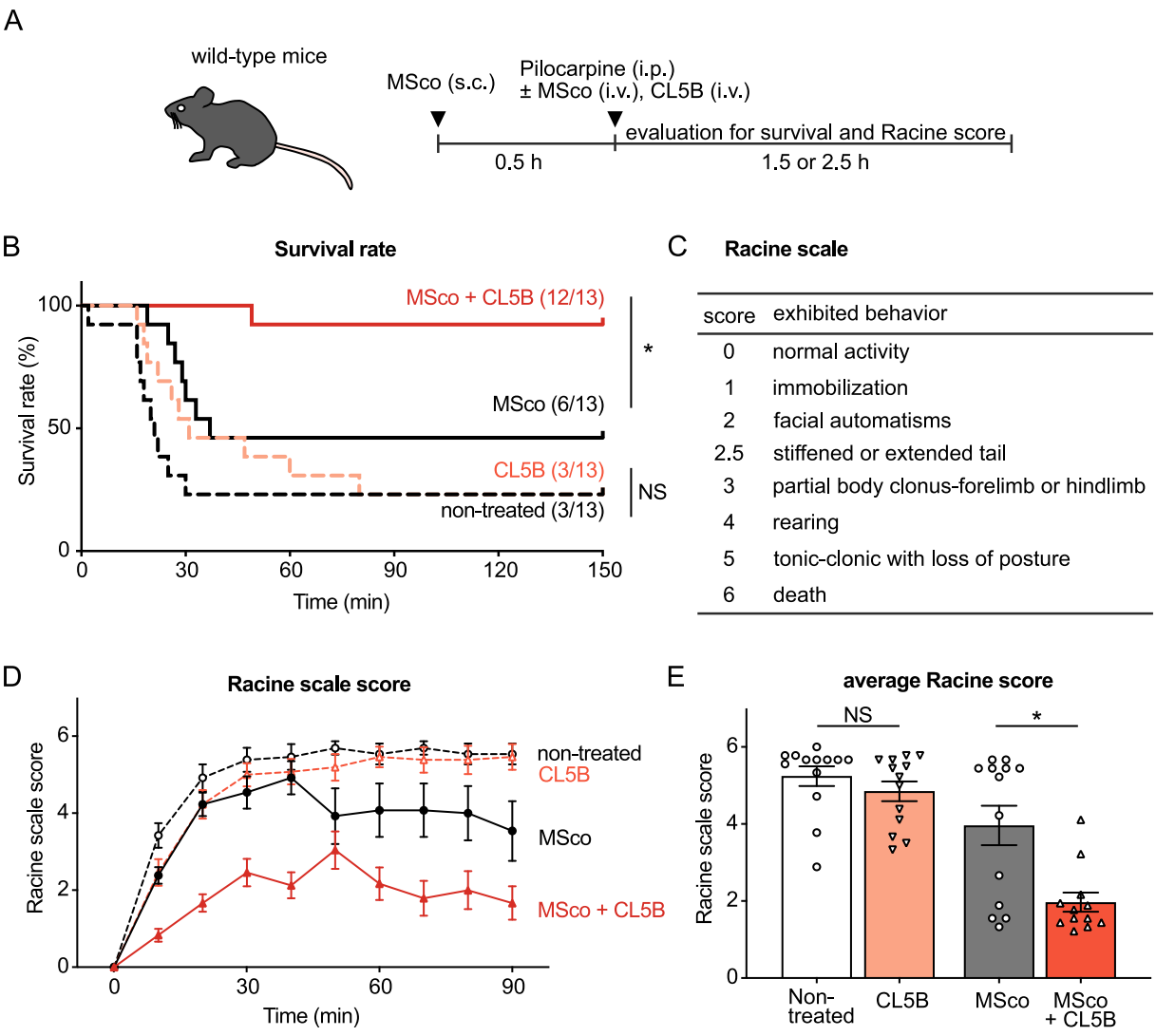

Fig. 6. CL5B-mediated methylscopolamine delivery to the brain alleviates epilepsy in an experimental mouse model.
(A) Schematic illustration of treatment assay using pilocarpine-induced mouse epilepsy model. Wild-type mice were pretreated with methylscoporamine (MSco) to inhibit pilocarpine-induced peripheral effects. The mice were then injected with pilocarpine to induce epilepsy and treated with MSco with or without CL5B. (B) Survival of epilepsy model mice with or without injecting MSco and/or CL5B ($n = 13$). P values were calculated using the log-rank test and then adjusted by Bonferroni correction. (C) Modified Racine scale scores. (D) Racine scale scores of epilepsy model mice with or without injection of MSco and/or CL5B. (E) Average Racine scale scores for each group in (D) ($n = 13$: non-treated, CL5B and MSco; $n = 12$: MSco + CL5B). *$P < 0.05$; NS: not significant by Mann–Whitney U test and then adjusted by Bonferroni correction.

blood vessels of peripheral organs such as the lung and spleen (Fig. S2A), raising the possibility that it might also affect these tissues. Notably, excessive anti-CLDN5 antibody treatment reportedly induces pulmonary hemorrhage and edema in mice and cynomolgus monkeys, respectively [24,25], highlighting the importance of evaluating potential peripheral vascular toxicity. However, in our analysis, CL5B-induced tracer leakage was the most pronounced in the brain (Fig. 5F), whereas changes in peripheral organs, such as the lungs, were modest. One possible explanation is that vascular permeability in non-brain organs is inherently higher owing to looser tight junctions and structural differences than in the brain; consequently, additional disruptions by CL5B do not elicit a marked increase. In contrast, the BBB relies heavily on CLDN5 to maintain its restrictive properties; therefore, CLDN5 inhibition is more readily visualized in the brain. These results suggest that CL5B acts preferentially at the BBB without causing overt peripheral toxicity under the tested conditions. Nevertheless, we acknowledge that systemic effects cannot be fully excluded. Further studies will be necessary to evaluate the safety of CL5B under high-dose or prolonged administration, examine possible interactions with other CLDN family members, and extend biodistribution and functional analyses in peripheral organs. Together, these considerations support the view that while CL5B represents a promising and relatively safe BBB modulator, comprehensive systemic safety evaluation remains an essential future direction.

A direct interaction between CLDN5 and small molecules has not been experimentally demonstrated because of technical difficulties. In this study, we demonstrated a direct interaction between CL5B and CLDN5 using an SPR assay, in which CLDN5-nanodiscs were employed as ligands, thereby preserving native conformation of CLDN5. Furthermore, in silico simulations identified the P2 near ECL2 of CLDN5 as a potential CL5B-binding pocket. This prediction offers a plausible explanation for the mechanism of CL5B action on CLDN5. Considering the location of the P2 site within ECL2, which is essential for the BBB function [21,26], together with the observation that CL5B treatment prevents the binding of M48, a conformation-sensitive antibody that targets ECL2, we infer that CL5B binds to the P2 pocket and induces a conformational change in ECL2, thereby loosening the tight junction sealing. To experimentally confirm this binding, further functional studies involving mutagenesis of ECL2 residues and structural analyses

of CLDN5–CL5B complexes will be necessary.

One possible explanation for why CL5B, despite its relatively low KD value (31.7–58.3 μM), can open the BBB is its transiently high blood concentration immediately after intravenous administration. Following injection, the blood concentration of CL5B increases rapidly but declines within approximately 20 min. Maximum concentration (C_{max}) and half-life time ($T_{1/2}$) were calculated to be 32.8 μM and 4.8 min, respectively (Fig. S3). Consistent with this pharmacokinetic profile, CL5B opens the BBB shortly after administration, and its activity is lost within 30 min. Thus, intravenous administration is required to transiently achieve a high blood concentration. This mode of administration likely enables CL5B to act only for a short period, limiting the duration of BBB opening.

Although a small-molecule CLDN5 modulator, M01, has been reported previously [15], its binding site and mechanism of action are completely different from those of CL5B. Direct interaction between M01 and CLDN5 was not experimentally demonstrated. An in silico prediction revealed that M01 primarily associates with ECL1 and with the outward-facing transmembrane surface of CLDN5, which is distinct from P2. Moreover, M01 opens the BBB over 3–48 h by reducing CLDN5 expression and requires hydroxypropyl-β-cyclodextrin (HPβCD) to improve its solubility. In contrast, CL5B rapidly and transiently opens the BBB within 30 min by altering CLDN5 localization without affecting its expression level, and does not require any solubility-enhancing additives. Taken together, CL5B is a novel small molecule-based CLDN5 modulator that directly binds to CLDN5, opens the BBB by inhibiting CLDN5, and facilitates drug delivery to the brain.

Several large molecules, such as peptides, proteolysis-targeting chimera (PROTAC), nucleic acids, and antibodies, have been proposed as drug candidates for brain diseases. However, delivering large molecules to the brain is difficult. Although previous studies have shown that CLDN5 modulators could promote the delivery of molecules less than approximately 1 kDa to the brain [9,13], delivery of larger molecules has not been carefully investigated. In this study, we found that CL5B could deliver vancomycin (a 1.4 kDa peptide) to the brain, which suggests the potential of CL5B to promote the delivery of various medium-sized drugs (0.5–2 kDa) to the brain. As CL5B was unable to deliver a larger molecule FD4 to the brain, alternative strategies are required for delivering large-sized drugs (>2 kDa) to the brain. A previous study showed that siRNA-mediated dual knockdown of CLDN5 and occludin promoted the brain penetration of a 3 kDa biotinylated dextran but not of a 10 kDa one [27]. Developing safer modulators that target occludin and other molecules may enable the delivery of large-sized drugs. The screening system and methodology used to identify CL5B may be applicable to small-molecule modulators targeting other intercellular adhesion molecules. Further studies on modulators targeting CLDN5 and other endothelial junction modulators should expand the possibilities of brain drug delivery via the paracellular pathway.

Paracellular drug delivery, which enables drug transport between endothelial cells by transiently opening the BBB, offers a simple and broadly applicable strategy compared with transcellular approaches that often require chemical modification or encapsulation of drugs. Although concerns have been raised about the safety of paracellular routes, recent advances in BBB modulation—particularly the use of focused ultrasound and small-molecule modulators—have begun to clarify the safety profile of transient BBB opening. Notably, CL5B induces a reversible opening of the BBB only for 30 min, which is much shorter than achieved with the modulators reported previously.

4. Conclusion

The CL5B-mediated brain drug delivery demonstrated in this study represents a safe, versatile, and efficient platform. It can potentially enhance the therapeutic efficacy of existing drugs for brain disorders and aid the development of novel therapeutics.

5. Materials and methods

5.1. Screening of CLDN5-binding molecules

An AlphaScreen assay system for screening CLDN5-binding compounds was developed using biotinylated-CLDN5 proteoliposomes and a human CLDN5 antibody M48 [22]. M48 is a mouse monoclonal antibody (IgG3) that specifically recognizes the structure of ECL2 of human CLDN5. For the control assay, biotinylated-CLDN1 proteoliposomes and a CLDN1 antibody 3A2 [28] were used. Biotinylated-CLDN proteoliposomes were prepared using a cell-free membrane protein synthesis system [29]. In this synthesis system, the synthesized membrane proteins are reconstituted into proteoliposomes with random orientation and high reconstitution efficiency, and maintain their structures and functions, as previously reported [30–32]. Using this assay system, we screened a core library of 9600 compounds provided by the Drug Discovery Initiative of the University of Tokyo. The samples and detection reagents were diluted in a solution containing 100 mM Tris-HCl (pH 8.0), 100 mM NaCl, and 1 mg/mL bovine serum albumin (BSA). All liquid samples were dispensed using FlexDrop Plus (Revvity). First, biotinylated-CLDN proteoliposomes were dispensed into a 384-well plate (Alpha Plate 384, Revvity) preloaded with the compound solution. Next, the CLDN antibody was added, which was followed by the addition of a solution containing AlphaScreen streptavidin-conjugated donor beads and Protein A-conjugated acceptor beads (Revvity). The reaction plates were incubated at 26 °C for at least 1 h. Finally, the AlphaScreen signals were measured using an EnVision plate reader (Revvity). The primary screening was conducted using 10 μM of the compounds ($n = 1$). In the secondary screening, tests were performed at compound concentrations of 1, 2, 5, 10, and 20 μM, with four replicates for each concentration. Inhibitory ratios were calculated from AlphaScreen signals using the following equation: Inhibitory ratio = $100 \times (1 - [\text{AlphaScreen signal}_{\text{compound}} - \text{negative-control signal}]/[\text{positive-control signal} - \text{negative-control signal}])$, where the positive-control signal refers to the average signal from reactions containing biotinylated-CLDN1 or CLDN5 proteoliposomes, the corresponding anti-CLDN antibody, and dimethyl sulfoxide (DMSO) ($n = 32$ wells per plate). The negative control was prepared by reversing the combination of antibody and proteoliposomes used in the positive control; the average signal in this case was also calculated from $n = 32$ wells per plate. Compounds that inhibited the binding between CLDN5 and the CLDN5 antibody, but not between CLDN1 and the CLDN1 antibody, were selected as candidate CLDN5 modulators.

5.2. CL5B, tracers, and drugs

The methods used for the synthesis and characterization of CL5B are described in the Supplementary Materials. The tracers and drugs used in this study are listed in Table S1.

5.3. Cells

Human dermal microvascular ECs (HDMECs) (Lonza) were cultured in EGM-2-MV medium (Lonza). The generation of MDCKII cell lines stably expressing human CLDN5 (MDCKII-hCLDN5) or mouse CLDN5 (MDCKII-mCLDN5) and a control cell line (MDCKII-mock) has been described previously [22]. MDCKII cells and a mouse brain EC line, bEnd.3 (ATCC), were maintained in Dulbecco's modified Eagle's medium (DMEM; Nacalai Tesque), supplemented with 10 % fetal bovine serum. All the cells were cultured under a humidified atmosphere with 5 % CO_2 at 37 °C.

5.4. Measurement of transepithelial/endothelial electrical resistance

MDCKII cells (8×10^4), HDMECs (4×10^4), or bEnd.3 cells (8×10^4) were seeded in cell culture inserts with a pore size of 0.4 μm (BD Falcon)

and cultured for 96 h to 10 days. The cell layers were then treated with CL5B (0–100 μM) or DMSO (as a control), and TEER was measured using a CellZscope system (NanoAnalytics). Data are expressed for each TEER value (Ω/cm^2) normalized to the values at time (t) = 0. For the knockdown experiments, HDMECs were transfected with siRNA targeting CLDN5 (D-011409-02; Dharmacon) or control siRNA (AllStars negative control (1027281); Qiagen) using RNAiMAX (Invitrogen) and seeded into cell culture inserts. For the TEER recovery assay, the medium was replaced with fresh medium without CL5B, 4 h after the CL5B treatment.

5.5. Measurement of the passage of tracers through the cell layer

Cell culture inserts seeded with MDCKII cells, HDMECs, or bEnd.3 cells were transferred to 24-well plates containing 1 mL of phenol red-free DMEM (Nacalai Tesque). The medium in the upper compartment was replaced with 0.4 mL of DMEM containing 10 μg/mL tracer (FITC (Fujifilm) or FNa (Wako Pure Chemical)). After 30 min, the tracer concentration in the lower compartment was measured using SpectraMax M5e (Excitation/Emission/cut off = 485/525/515 nm; Molecular Devices). The apparent permeability (Papp) coefficients (in cm/s) were calculated using the following equation: Papp = (lower compartment volume × tracer concentration in the sample)/(assay time × surface area of the culture inserts × initial tracer concentration).

5.6. Surface plasmon resonance assay

CLDN5- and Control-nanodiscs were prepared by cell-free synthesis using the NanoDisc BD Kit (CellFree Sciences). The cDNA encoding CLDN5 with a C-terminal His-tag was cloned into the pEU-E01-GW plasmid (CellFree Sciences). To enable biotinylation of nanodiscs, the His-tag sequence of pEU-E01-MSP (provided with the NanoDisc BD Kit) was replaced with an Avi-tag by inverse PCR and seamless cloning. CLDN5-His, Avi-MSP1E3D1, and His-MSP1E3D1 mRNAs were then prepared by in vitro transcription. For the translation of CLDN5-nanodiscs, the reaction mixture was prepared by combining 167 μL of WEPRO7240ND, 20 μL of creatine kinase (1 mg/mL), 111 μL of Avi-tag-MSP1E3D1 mRNA, 58 μL of CLDN5-His mRNA, 24 μL of biotin (60 μM), 20 μL of cell-free synthesized BirA, and 100 μL of Asolectin (50 mg/mL). The reaction mixture for Control-nanodiscs comprised 167 μL of WEPRO7240ND, 20 μL of creatine kinase (1 mg/mL), 60 μL each of Avi-tag-MSP1E3D1 and His-MSP1E3D1 mRNAs, 24 μL of biotin (60 μM), 20 μL of cell-free synthesized BirA, 100 μL of Asolectin (50 mg/mL), and 49 μL of SUB-AMIX SGC solution. A Slide-A-Lyzer MINI Dialysis Device (10 K MWCO, Thermo Fisher Scientific) was inserted into a tube containing the SUB-AMIX SGC solution, and 2 mL of SUB-AMIX SGC was added to the cup. Subsequently, the translation reaction mixture was layered on the bottom of the dialysis cup. After a 20-h reaction at 16 °C, the contents of the inner cup were collected.

To purify nanodiscs, imidazole (5 mM) and 15 μL of Ni Sepharose HP (Cytiva) were added to a translation reaction mixture. The mixture was mixed gently by rotating at 4 °C for 1 h. The resin was collected by a MicroSpin Empty Column (Cytiva), washed with washing buffer (50 mM Hepes-NaOH, 30 mM imidazole, 300 mM NaCl), and eluted with elution buffer (50 mM Hepes-NaOH, 500 mM imidazole, 300 mM NaCl). The eluted nanodiscs were buffer-exchanged with HBS-N buffer (10 mM Hepes-NaOH, pH 7.22, 150 mM NaCl) using a PD MiniTrap G-25 column. The purity of the nanodiscs was confirmed by sodium dodecyl sulfate-polyacrylamide gel electrophoresis (SDS-PAGE) followed by Coomassie Brilliant Blue staining. Avi-tag biotinylation was verified using western blotting.

SPR measurement was performed using a Biacore 1S+ instrument (Cytiva). For ligand immobilization, PBS (137 mM NaCl, 2.7 mM KCl, 1.5 mM KH_2PO_4, 8.1 mM Na_2HPO_4) was used as the running buffer. Approximately 3,000–3,500 RU of CLDN5-nanodiscs and Control-nanodiscs were immobilized on the measurement and reference cells of a Series S Sensor Chip SA (Cytiva), respectively. The running buffer for affinity assay was PBS containing 2 % DMSO. The CL5B/DMSO stock solution was diluted with PBS to achieve a final DMSO concentration of 2 %, and serial dilutions were prepared using the running buffer. Each analyte was injected at 30 μL/min at 25 °C, with association and dissociation times of 60 s each. Sensorgrams were referenced by subtracting the response in the reference cell. The steady-state response was defined as the median response between 25 s and 35 s after the injection and plotted to generate a saturation curve. K_D and *R*max values were obtained by fitting the saturation data to a 1:1 binding model using nonlinear least-squares fitting in the R statistical software. [33]

5.7. Molecular dynamics simulations

The putative structure of hCLDN5 was retrieved from the AlphaFold Protein Structure database (https://alphafold.ebi.ac.uk, ID: AF-O00501-F1-v4), and the unstructured regions (192–218) were removed. To predict the drug-binding pockets on the surface of CLDN5, the MolSite method was applied after predicting and adding hydrogen atoms to CLDN5 using the AddH program in the myPresto software suite. A docking model between CL5B and hCLDN5 was constructed based on the predicted drug-binding pockets using myPresto. To evaluate the binding complex, molecular dynamics (MD) simulations were conducted using the GROMACS software for a total simulation time of 200 ns. The complex was first solvated in water under physiological ion concentrations (Na^+: 154 mM; K^+: 4 mM; Cl^-: 158 mM). Thereafter, energy minimization was performed with 5,000 iterations for both the steepest descent and conjugate gradient methods. For equilibration, the system underwent NVT-MD (constant volume and temperature) for 400 ps at 300 K with main-chain constraints, followed by NPT-MD (constant pressure and temperature) for 400 ps at 310 K, with main-chain constraints. The production MD simulation under NPT conditions was then run for 200 ns at 310 K. Trajectory data were visualized using the Prism10 software (GraphPad Software).

5.8. Immunofluorescence staining and image analysis

HDMECs were cultured on a chamber slide (Thermo Fisher Scientific) in the presence or absence of CL5B for 10 h. Thereafter, the cells were fixed with 4 % paraformaldehyde and blocked with 1 % BSA in PBS. These cells were incubated with the CLDN5 antibody (R9 [22]; 5 ng/μL) followed by incubation with a secondary antibody conjugated with Alexa Fluor 546 (Thermo Fisher Scientific). The slides were mounted using VECTASHIELD Mounting Medium with 4′,6-diamidino-2-phenylindole (DAPI; Vector Laboratories) and analyzed using BZ-X700 (KEYENCE) or a Nikon AX R MP with NSPARC super-resolution confocal laser scanning microscope (Nikon) equipped with a × 60/1.42 NA oil-immersion objective lens (2048 × 2048). The CLDN5 continuity was quantified using the obtained images with ImageJ/Fiji [34]. Junctional areas were delineated by manually outlining each cell, followed by enlarging and shrinking the outline by 2 pixels to define the region containing the junctions. To assess the continuity of the CLDN5 structure, the CLDN5 channel was converted to a binary image with a threshold range of 31–255. The number of pixels within the junctional area was then measured. Finally, the CLDN5 continuity was calculated as a percentage of pixels with an intensity value of 255 relative to the total number of pixels in the junctional area.

5.9. Western blot analysis

HDMEC extract was prepared using a sample buffer (50 mM Tris-HCl (pH 6.8), 2 % SDS, 6.6 % 2-mercaptoethanol, 10 % glycerol, and 0.002 % bromophenol blue). The proteins in the cell extract were separated using SDS-PAGE and transferred onto polyvinylidene fluoride membranes. The membranes were incubated with primary antibodies against hCLDN5 (4C3C2, Thermo Fisher Scientific) or GAPDH (6C5, Merck Millipore) and subsequently with horseradish peroxidase-conjugated

secondary antibodies. Immunoreactive bands were detected using an ImageQuant LAS4010 system (GE Healthcare). The antibodies used in this study are listed in Table S2.

5.10. Animals

All animal experiments were approved by the ethics committee of the University of Osaka (approval numbers Douyaku 30–11-4, R05–26, and R01–3-2) and were performed in accordance with the relevant guidelines and regulations. Human CLDN5 knock-in mice (hCLDN5-KI mice) were generated as described previously [25]. Wild-type C57BL/6 mice were purchased from Shimizu Laboratory.

5.11. Quantitative reverse transcription-polymerase chain reaction

Organs were harvested from wild-type and hCLDN5-KI mice (male, 7–9 weeks old). Total RNA from the organs and ECs was prepared using the RNeasy Mini Kit (Qiagen), FastGene RNA Basic Kit (NIPPON Genetics), or ISOGEN (NIPPON GENE). RNA was reverse transcribed using Superscript VILO Master Mix (Invitrogen). Quantitative reverse-transcription-polymerase chain reaction (qRT-PCR) was performed using the obtained cDNA, QuantiTect SYBR Green PCR Kit (Qiagen), and specific primers (Table S3) on a CFX384 Touch Real-Time PCR Detection System (Bio-Rad). The relative quantitation of target mRNA levels was performed using the $2^{-\Delta\Delta Ct}$ method. The expression levels of the genes were normalized to those of *GAPDH*.

5.12. Analysis of hCLDN5-KI mice injected with fluorescein-conjugated antibodies

The CLDN5 antibody (R9) and control IgG (Sigma-Aldrich) were labeled using a Fluorescein labeling kit-NH_2 (Dojindo Molecular Technologies). Briefly, each antibody was mixed with a reaction buffer containing NH_2-reactive fluorescein and collected via filtration. Fluorescein-conjugated CLDN5 antibody (3 mg/kg) was intravenously injected into hCLDN5-KI mice (female, 9 weeks old). After 1 h, the mice were perfused with 10 mL of PBS containing 2 mM EDTA and Dylight 594-conjugated tomato lectin (0.1 mg/mouse; Vector laboratories). The brain was harvested from the mice, and frozen sections (5 μm) were prepared. The sections were fixed with 4 % paraformaldehyde for 30 min and analyzed using a BZ-X700 microscope.

5.13. Brain delivery assay using fluorescent tracers

For the antibody assays, hCLDN5-KI mice (male, 7–9 weeks old) were intravenously injected with the CLDN5 antibody (R9; 3.5 mg/kg) or control IgG (3.5 mg/kg). After 1 h, the mice were injected with 10 mg/mouse fluorescent tracers, FNa (376 Da) or FITC-labeled dextran 4 kDa (FD4; Sigma-Aldrich). After 1 h, the mice were perfused with PBS containing 2 mM EDTA, and their brain was harvested. The brain was homogenized in 1 mL PBS, incubated for 16–48 h, and centrifuged (17,500 ×*g*, 5 min). Fluorescence intensities in the supernatant were measured using a SpectraMax M5e (Excitation/Emission/cut off = 485/525/515 nm). In the assays with CL5B, hCLDN5-KI or wild-type C57BL/6 mice (male, 7–10 weeks old) were injected with CL5B (2.5 mg/kg) in PBS containing 10 % DMSO. Immediately (0 h) or 0.5 h later, the mice were injected with FNa or FD4 (10 mg/mouse), perfused, and analyzed in a similar manner.

5.14. Measurement of CL5B concentration in blood samples

CL5B (2.5 mg/kg body weight, dissolved in PBS containing 10 % DMSO) was administered intravenously to wild-type mice. Whole blood samples were collected at 1–16 min after administration. Measurement samples were prepared by precipitating the proteins with acetonitrile. The concentrations of CL5B in the samples were analyzed using an ACQUITY UPLC system (Waters Corporation), equipped with a BEH C18 column (1.7 μm, 2.1 × 50 mm, Waters), coupled to an Xevo TQ-S mass spectrometer (Waters). Liquid chromatography-tandem mass spectrometry (LC-MS/MS) data were acquired under the following conditions: mobile phase A = 0.1 % formic acid in water; mobile phase B = 0.1 % formic acid in acetonitrile; gradient elution: 0 min – 2 % B, 1.8 min – 98 % B; and flow rate: 0.5 mL/min.

5.15. Brain delivery assay using Hoechst 33528

hCLDN5-KI mice (male, 9 weeks old) were intravenously injected with Dylight594-conjugated tomato lectin (0.1 mg/mouse). After 5 min, the mice were intravenously injected with CL5B (2.5 mg/kg; in PBS containing 10 % DMSO) and Hoechst 33258 (1 mg/mouse; Invitrogen) and perfused with PBS containing 2 mM EDTA, and their brain was harvested. The prepared frozen sections (5 μm) were mounted using Glycerol and analyzed using a BZ-X700.

5.16. Brain delivery assay using methylscopolamine and vancomycin

C57BL/6 mice (male, 8 weeks old) were intravenously injected with MSco (2 mg/kg; Sigma-Aldrich) or vancomycin (100 mg/kg; Wako), with or without CL5B (2.5 mg/kg). After 30 min, the mice were perfused with PBS, and their brain was harvested. The brain was homogenized with four times its weight of cold water, and 25 μL of the homogenate was mixed with 50 μL of acetonitrile. The mixture was then centrifuged (1,900 ×*g*, 10 min), and the supernatants were used to quantify MSco and vancomycin using LC-MS/MS.

LC-MS/MS analyses were performed on an ACQUITY Premier UPLC (Waters) with a cooled autosampler set at 15 °C and a column oven at 60 °C, coupled to a Xevo TQ Absolute triple quadrupole mass spectrometer (Waters) equipped with an electrospray ionization source. Chromatographic separation was performed on an ACQUITY UPLC BEH C18 column (1.7 μm, 50 mm × 2.1 mm; Waters). Mobile phase A was water with 0.1 % formic acid, and mobile phase B was acetonitrile with 0.1 % formic acid. The flow rate was set at 0.5 mL/min, with an injection volume of 5 μL. The gradient program started at 2 % B, increased to 98 % B over 1.8 min, then returned to 2 % B in 0.7 min, followed by re-equilibration at 2 % B for 2.5 min (total run time 5 min). MS was operated in ESI positive mode with a capillary voltage of 3 kV, cone voltage of 20 V, desolvation temperature of 400 °C, cone gas flow of 150 L/h, and desolvation gas flow of 600 L/h. MSco and vancomycin were quantified using multiple reaction monitoring with the following transitions: MSco, *m/z* 319.13 → 153.17 (cone voltage of 35 V, collision energy of 25 eV, and dwell time of 0.05 ms); vancomycin, m/z 725.76 → 100.43 (cone voltage of 35 V, collision energy of 25 eV, and dwell time of 0.05 ms). Their expected retention times were 1.23 and 1.10 min, respectively. An internal standard, daidzein (m/z 255.00 → 198.99), was included in all samples.

5.17. Pilocarpine-induced epilepsy model

Wild-type mice (male, 8 weeks old) were subcutaneously injected with MSco (1 mg/kg). After 30 min of injection, pilocarpine (400 mg/kg; Wako) was intraperitoneally injected, followed by an intravenous injection of MSco (2 mg/kg) with or without CL5B (2.5 mg/kg). The behaviors of the mice were recorded, and the survival and severity of epilepsy were scored according to a modified Racine scale [35,36].

5.18. Statistical analysis

Data are expressed as mean values ± standard error (s.e.m.) and graphically presented as scatter plots. Normality was tested using the Shapiro–Wilk test. For samples with a normal distribution, *P*-values were calculated using the unpaired Welch's *t*-test between two samples and one-way analysis of variance (ANOVA), followed by Bonferroni's,

Tukey's, or Dunnett's tests among more than three samples. For samples with a non-normal distribution, *P*-values were calculated using the Mann–Whitney *U* test between two samples and the Mann–Whitney *U* test followed by the Bonferroni correction or the Kruskal–Wallis test among more than three samples. For survival curves, *P*-values were calculated using the log-rank test and adjusted with Bonferroni's correction. All statistical analyses were performed using the Prism 10 software. Statistical significance of the differences in means was determined using the tests indicated in the figure legends. A *P*-value <0.05 was considered statistically significant.

Supplementary data to this article can be found online at https://doi.org/10.1016/j.jconrel.2025.114314.

Author contribution

S.I., A.S., and K.M. performed qRT-PCR analysis. R.F., K.M., Y.H., K. T., H.T., and M.K. performed experiments using hCLDN5 antibodies. S.I., A.S., R.F., K.M., and Y. Ikemi performed the brain delivery and in vivo assays. K.S., R.F., H.T., and M.K. screened the small molecules. J.T., S.T., and T.H. synthesized CL5B. S.I., K.S., A.S., R.F., and K.M. measured the TEER and tracer passage. S.I., A.S., and Y. Ikeda performed molecular dynamics simulations. S.I., K.S., A.S., and K.M. performed the immunofluorescence staining, western blotting, and image analysis. S.I., A.S., N.K., and T.K. analyzed the brain drug delivery. S.I. and A.S. performed experiments using the mouse epilepsy model. N.H., T.D., S.N., S.T., M. O., and Y.F. interpreted the data. S.I., K.S., T.H., H.T., M.K., and Y.O. wrote the manuscript.

Declaration of competing interest

A patent application has been filed for CL5B, which exhibits blood–brain barrier (BBB)–modulating effects as described in this manuscript (PCT/JP2025/018138). The authors declare no other conflicts of interest.

Acknowledgments

We thank Drs. Atsushi Kasai, Hitoshi Hashimoto, Yukio Ago, Yasuo Tsutsumi, Kazuma Higashisaka, Hiroshi Aoyama, Toshiyuki Kume, and Mariko Okada for their helpful suggestions and technical assistance. This work was fully or partially supported by the Program for Creating Start-ups from Advanced Research and Technology from the Japan Science and Technology Agency, the Platform Project for Supporting in Drug Discovery and Life Science Research (Platform for Drug Discovery, Informatics, and Structural Life Science) from AMED/MEXT, the JSPS KAKENHI (JP17K19487, JP22H04922, JP22K19377, JP23H02629, and JP23K27320), AMED (JP24ama121054, JP24ama121052, and JP24ama121043), SENSHIN Medical Research Foundation, Takeda Science Foundation, Shionogi Infectious Disease Research Promotion, and the Nippon Foundation–Osaka University Project for Infectious Disease Prevention.

Data availability

Data will be made available on request.

References

[1] J.J. Lochhead, J. Yang, P.T. Ronaldson, T.P. Davis, Structure, function, and regulation of the blood-brain barrier tight junction in central nervous system disorders, Front. Physiol. 11 (2020) 914.
[2] C. Zihni, C. Mills, K. Matter, M.S. Balda, Tight junctions: from simple barriers to multifunctional molecular gates, Nat. Rev. Mol. Cell Biol. 17 (2016) 564–580.
[3] O.R. Colegio, C. Van Itallie, C. Rahner, J.M. Anderson, Claudin extracellular domains determine paracellular charge selectivity and resistance but not tight junction fibril architecture, Am. J. Phys. Cell Phys. 284 (2003) C1346–C1354.
[4] N. Gehne, R.F. Haseloff, I.E. Blasig, Identity crisis in the PMP-22/EMP/MP20/Claudin superfamily (Pfam00822), Tissue Barriers 3 (2015) e1089680.
[5] H. Suzuki, T. Nishizawa, K. Tani, Y. Yamazaki, A. Tamura, R. Ishitani, N. Dohmae, S. Tsukita, O. Nureki, Y. Fujiyoshi, Crystal structure of a claudin provides insight into the architecture of tight junctions, Science 344 (2014) 304–307.
[6] G. Krause, L. Winkler, C. Piehl, I. Blasig, J. Piontek, S.L. Muller, Structure and function of extracellular claudin domains, Ann. N. Y. Acad. Sci. 1165 (2009) 34–43.
[7] C. Piehl, J. Piontek, J. Cording, H. Wolburg, I.E. Blasig, Participation of the second extracellular loop of claudin-5 in paracellular tightening against ions, small and large molecules, Cell. Mol. Life Sci. 67 (2010) 2131–2140.
[8] C. Greene, J. Kealy, M.M. Humphries, Y. Gong, J. Hou, N. Hudson, L.M. Cassidy, R. Martiniano, V. Shashi, S.R. Hooper, G.A. Grant, P.F. Kenna, K. Norris, C. K. Callaghan, M.D. Islam, S.M. O'Mara, Z. Najda, S.G. Campbell, J.S. Pachter, J. Thomas, N.M. Williams, P. Humphries, K.C. Murphy, M. Campbell, Dose-dependent expression of claudin-5 is a modifying factor in schizophrenia, Mol. Psychiatry 23 (2018) 2156–2166.
[9] T. Nitta, M. Hata, S. Gotoh, Y. Seo, H. Sasaki, N. Hashimoto, M. Furuse, S. Tsukita, Size-selective loosening of the blood-brain barrier in claudin-5-deficient mice, J. Cell Biol. 161 (2003) 653–660.
[10] E. Vazquez-Liebanas, G. Mocci, W. Li, B. Lavina, A. Reddy, C. O'Connor, N. Hudson, Z. Elbeck, I. Nikoloudis, K. Gaengel, M. Vanlandewijck, M. Campbell, C. Betsholtz, M.A. Mae, Mosaic deletion of claudin-5 reveals rapid non-cell-autonomous consequences of blood-brain barrier leakage, Cell Rep. 43 (2024) 113911.
[11] Y. Li, C. Wang, L. Zhang, B. Chen, Y. Mo, J. Zhang, Claudin-5a is essential for the functional formation of both zebrafish blood-brain barrier and blood-cerebrospinal fluid barrier, Fluids Barriers CNS 19 (2022) 40.
[12] A. Parodi, M. Rudzinska, A.A. Deviatkin, S.M. Soond, A.V. Baldin, A. A. Zamyatnin Jr., Established and emerging strategies for drug delivery across the blood-brain barrier in brain cancer, Pharmaceutics 11 (2019).
[13] M. Campbell, A.S. Kiang, P.F. Kenna, C. Kerskens, C. Blau, L. O'Dwyer, A. Tivnan, J.A. Kelly, B. Brankin, G.J. Farrar, P. Humphries, RNAi-mediated reversible opening of the blood-brain barrier, J. Gene Med. 10 (2008) 930–947.
[14] M. Campbell, F. Hanrahan, O.L. Gobbo, M.E. Kelly, A.S. Kiang, M.M. Humphries, A. T. Nguyen, E. Ozaki, J. Keaney, C.W. Blau, C.M. Kerskens, S.D. Cahalan, J. J. Callanan, E. Wallace, G.A. Grant, C.P. Doherty, P. Humphries, Targeted suppression of claudin-5 decreases cerebral oedema and improves cognitive outcome following traumatic brain injury, Nat. Commun. 3 (2012) 849.
[15] O. Breitkreuz-Korff, C. Tscheik, G. Del Vecchio, S. Dithmer, W. Walther, A. Orthmann, H. Wolburg, R.F. Haseloff, L. Schroder, I.E. Blasig, L. Winkler, M01 as a novel drug enhancer for specifically targeting the blood-brain barrier, J. Control. Release 338 (2021) 137–148.
[16] Z. Liao, Z. Yang, A. Piontek, M. Eichner, G. Krause, L. Li, J. Piontek, J. Zhang, Specific binding of a mutated fragment of *Clostridium perfringens* enterotoxin to endothelial claudin-5 and its modulation of cerebral vascular permeability, Neuroscience 327 (2016) 53–63.
[17] J. Protze, M. Eichner, A. Piontek, S. Dinter, J. Rossa, K.G. Blecharz, P. Vajkoczy, J. Piontek, G. Krause, Directed structural modification of *Clostridium perfringens* enterotoxin to enhance binding to claudin-5, Cell. Mol. Life Sci. 72 (2015) 1417–1432.
[18] L. Chen, R. Sutharsan, J.L. Lee, E. Cruz, B. Asnicar, T. Palliyaguru, J. M. Wasielewska, A. Gaudin, J. Song, G. Leinenga, J. Gotz, Claudin-5 binder enhances focused ultrasound-mediated opening in an in vitro blood-brain barrier model, Theranostics 12 (2022) 1952–1970.
[19] W. Neuhaus, A. Piontek, J. Protze, M. Eichner, A. Mahringer, E.A. Subileau, I. M. Lee, J.D. Schulzke, G. Krause, J. Piontek, Reversible opening of the blood-brain barrier by claudin-5-binding variants of *Clostridium perfringens* enterotoxin's claudin-binding domain, Biomaterials 161 (2018) 129–143.
[20] S. Dithmer, C. Staat, C. Muller, M.C. Ku, A. Pohlmann, T. Niendorf, N. Gehne, P. Fallier-Becker, A. Kittel, F.R. Walter, S. Veszelka, M.A. Deli, R. Blasig, R. F. Haseloff, I.E. Blasig, L. Winkler, Claudin peptidomimetics modulate tissue barriers for enhanced drug delivery, Ann. N. Y. Acad. Sci. 1397 (2017) 169–184.
[21] M. Trevisani, A. Berselli, G. Alberini, E. Centonze, S. Vercellino, V. Cartocci, E. Millo, D.Z. Ciobanu, C. Braccia, A. Armirotti, F. Pisani, F. Zara, V. Castagnola, L. Maragliano, F. Benfenati, A claudin5-binding peptide enhances the permeability of the blood-brain barrier in vitro, Sci. Adv. 11 (2025) eadq2616.
[22] Y. Hashimoto, K. Shirakura, Y. Okada, H. Takeda, K. Endo, M. Tamura, A. Watari, Y. Sadamura, T. Sawasaki, T. Doi, K. Yagi, M. Kondoh, Claudin-5-binders enhance permeation of solutes across the blood-brain barrier in a mammalian model, J. Pharmacol. Exp. Ther. 363 (2017) 275–283.
[23] Y. Hashimoto, W. Zhou, K. Hamauchi, K. Shirakura, T. Doi, K. Yagi, T. Sawasaki, Y. Okada, M. Kondoh, H. Takeda, Engineered membrane protein antigens successfully induce antibodies against extracellular regions of claudin-5, Sci. Rep. 8 (2018) 8383.
[24] K. Tachibana, Y. Hashimoto, K. Shirakura, Y. Okada, R. Hirayama, Y. Iwashita, I. Nishino, Y. Ago, H. Takeda, H. Kuniyasu, M. Kondoh, Safety and efficacy of an anti-claudin-5 monoclonal antibody to increase blood-brain barrier permeability for drug delivery to the brain in a non-human primate, J. Control. Release 336 (2021) 105–111.
[25] R. Hashimoto, J. Takahashi, K. Shirakura, R. Funatsu, K. Kosugi, S. Deguchi, M. Yamamoto, Y. Tsunoda, M. Morita, K. Muraoka, M. Tanaka, T. Kanbara, S. Tanaka, S. Tamiya, N. Tokunoh, A. Kawai, M. Ikawa, C. Ono, K. Tachibana, M. Kondoh, M. Obana, Y. Matsuura, A. Ohsumi, T. Noda, T. Yamamoto, Y. Yoshioka, Y.S. Torisawa, H. Date, Y. Fujio, M. Nagao, K. Takayama, Y. Okada, SARS-CoV-2 disrupts respiratory vascular barriers by suppressing Claudin-5 expression, Sci. Adv. 8 (2022) eabo6783.

[26] A. Berselli, G. Alberini, F. Benfenati, L. Maragliano, Computational assessment of different structural models for Claudin-5 complexes in blood-brain barrier tight junctions, ACS Chem. Neurosci. 13 (2022) 2140–2153.
[27] J. Keaney, D.M. Walsh, T. O'Malley, N. Hudson, D.E. Crosbie, T. Loftus, F. Sheehan, J. McDaid, M.M. Humphries, J.J. Callanan, F.M. Brett, M.A. Farrell, P. Humphries, M. Campbell, Autoregulated paracellular clearance of amyloid-beta across the blood-brain barrier, Sci. Adv. 1 (2015) e1500472.
[28] M. Fukasawa, S. Nagase, Y. Shirasago, M. Iida, M. Yamashita, K. Endo, K. Yagi, T. Suzuki, T. Wakita, K. Hanada, H. Kuniyasu, M. Kondoh, Monoclonal antibodies against extracellular domains of claudin-1 block hepatitis C virus infection in a mouse model, J. Virol. 89 (2015) 4866–4879.
[29] W. Zhou, H. Takeda, Cell-free production of proteoliposomes for functional analysis and antibody development targeting membrane proteins, J. Vis. Exp. 163 (2020). https://app.jove.com/v/61871/cell-free-production-proteoliposomes-for-functional-analysis-antibody.
[30] E. Arimitsu, T. Ogasawara, H. Takeda, T. Sawasaki, Y. Ikeda, Y. Hiasa, K. Maeyama, The ligand binding ability of dopamine D1 receptors synthesized using a wheat germ cell-free protein synthesis system with liposomes, Eur. J. Pharmacol. 745 (2014) 117–122.
[31] R. Nishiguchi, T. Tanaka, J. Hayashida, T. Nakagita, W. Zhou, H. Takeda, Evaluation of cell-free synthesized Human Channel proteins for in Vitro Channel research, Membranes (Basel) 13 (2022).
[32] H. Takeda, T. Ogasawara, T. Ozawa, A. Muraguchi, P.J. Jih, R. Morishita, M. Uchigashima, M. Watanabe, T. Fujimoto, T. Iwasaki, Y. Endo, T. Sawasaki, Production of monoclonal antibodies against GPCR using cell-free synthesized GPCR antigen and biotinylated liposome-based interaction assay, Sci. Rep. 5 (2015) 11333.
[33] J.M.C. Douglas, M. Bates, Nonlinear models, in: T.J. Chambers (Ed.), Statistical Models in S, J. M. A. H, Wadsworth & Brooks/Cole, Pacific Grove, CA, 1992, pp. 421–460.
[34] J. Schindelin, I. Arganda-Carreras, E. Frise, V. Kaynig, M. Longair, T. Pietzsch, S. Preibisch, C. Rueden, S. Saalfeld, B. Schmid, J.Y. Tinevez, D.J. White, V. Hartenstein, K. Eliceiri, P. Tomancak, A. Cardona, Fiji: an open-source platform for biological-image analysis, Nat. Methods 9 (2012) 676–682.
[35] M.N. Arshad, J.R. Naegele, Induction of temporal lobe epilepsy in mice with pilocarpine, Bio-Protoc. 10 (2020) e3533.
[36] T.D. Nguyen, M. Ishibashi, A.S. Sinha, M. Watanabe, D. Kato, H. Horiuchi, H. Wake, A. Fukuda, Astrocytic NKCC1 inhibits seizures by buffering Cl(−) and antagonizing neuronal NKCC1 at GABAergic synapses, Epilepsia 64 (2023) 3389–3403.